ICTAM 2024

Features of turbulent boundary layers in heated concentric coaxial pipe flow at high Reynolds and low Prandtl numbers

Brandenburgische Technische Universität Cottbus - Senftenberg

Pei-Yun Tsai [1,2], Heiko Schmidt [1,2] and Marten Klein [1,2]

Energie-Innovationszentrum Cottbus

[1] Numerical Fluid and Gas Dynamics, Brandenburg University of Technology, Cottbus, Germany

[2] Scientific Computing Lab (SCL), Energy Innovation Center (EIZ), Brandenburg University of Technology, Cottbus, Germany

Introduction and Motivation

- Concentric coaxial (annular) pipe flow has been studied numerically (**Figure 1**) and experimentally [1]
- Dependencies of **radius ratio** [2,3,4], **Reynolds number** [4], **Prandtl number** [5], **heat flux ratio** [6], and **boundary condition** [4] have been investigated previously.
- Annular pipe flow coupling with heat (scalar) transfer under high Reynolds numbers and small radius ratios cases have **not** yet been discussed.
- Resolving the boundary layer at the inner remains challenging due to high resolution requirements.

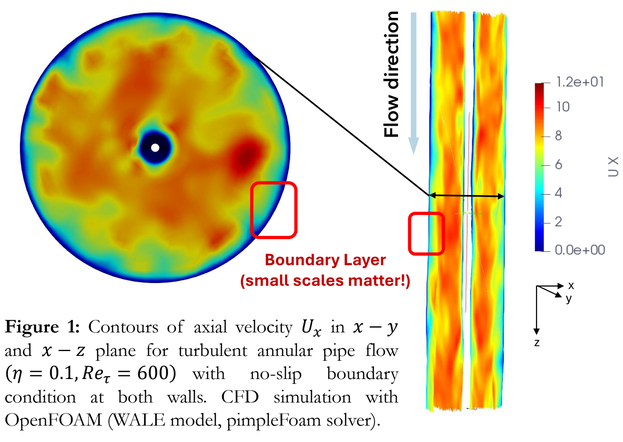

Figure 1: Contours of axial velocity U_x in $x-y$ and $x-z$ plane for turbulent annular pipe flow ($\eta = 0.1, Re_\tau = 600$) with no-slip boundary condition at both walls. CFD simulation with OpenFOAM (WALE model, pimpleFoam solver).

Main objectives

- Utilizing a computationally efficient stochastics turbulence model as a standalone tool to simulate heated annular pipe flows
- Rigorous theoretical analysis of thermal and momentum boundary layer over spanwise curved wall
- Investigate high Reynolds number and low Prandtl number

Overview of ODT model formulation and calibration

One-dimensional turbulence (ODT) model [7] is a dimensionally reduced flow model that can be economically utilized as a stand-alone tool. ODT offers **full-scale resolution** of the instantaneous velocity and temperature profile along a 1D radial coordinate (**Figure 2**) by modeling the advection terms using a stochastic process.
Here, we consider pressure-driven (Poiseuille flow) annular pipe flow with no-slip and constant heat flux boundary conditions on the inner and outer cylindrical walls. The governing equations can be written as [8,9] :

$$\frac{\partial u_i}{\partial t} + \sum_{t_e} \varepsilon_u \, \delta(t - t_e) = \frac{1}{r}\frac{\partial}{\partial r}\left(r\nu \frac{\partial u_i}{\partial r}\right) - \frac{1}{\rho}\frac{dP}{dx}\delta_{1i} \quad (1) \qquad \frac{\partial \Theta}{\partial t} + \sum_{t_e} \varepsilon_\Theta \, \delta(t - t_e) = \frac{1}{r}\frac{\partial}{\partial r}\left(r\alpha \frac{\partial \Theta}{\partial r}\right) + u\frac{dT_m}{dx} \quad (2)$$

where $u_i (i = x, r, \theta)$ represents the cylindrical components of the model-resolved instantaneous velocity vector, Θ the perturbation temperature relative to the axially increasing mean temperature T_m, due to dT_m/dx is constant, t_e the stochastically sampled times of eddy events affecting the velocity and scalar by ε_u and ε_Θ, and $\delta(t - t_e)$ is the Dirac delta function. Eddy events are modeled by spatial mappings in the form of radial 1-D generalized baker's maps [8].

ODT model parameters ($\alpha = 1/6$, $C = 5$ and $Z = 400$ are used here [10])
- α : Energy Distribution parameter
- C : Eddy frequency parameter
- Z : Viscous penalty parameter

- Eddy length: l ← randomly choose ← Use spatial mapping
- Eddy rate: $\frac{1}{\tau} = \sqrt{\frac{1}{l^6}(u_K^2 + v_K^2 + w_K^2) - Z\frac{\nu^2}{l^4}}$
- Eddy rate distribution: $\lambda(l, y_0; t) = \frac{C}{l^2 \tau(l, y_0; t)}$

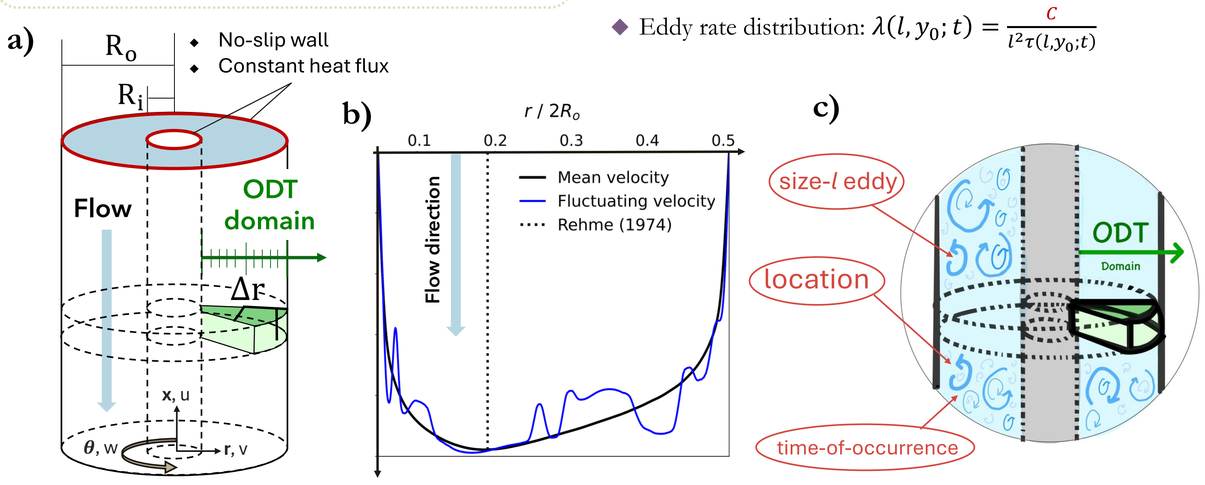

Figure 2: (a) Schematic of the annular pipe flow configuration with the wedge-like radially oriented ODT domain (line) is sketched. No-slip and constant heat flux boundary conditions are prescribed at the annulus walls. **(b)** The mean and instantaneous radial profile of the axial velocity component with $\eta = R_i/R_o = 0.1$ and $Re_{Dh} = \frac{D_h U_b}{\nu} = \frac{2(R_o - R_i)U_b}{\nu} = 17700$. The dotted line indicates an empirical formula for the location of maximum axial velocity from [1]. **(c)** Diagram of eddy events characterized by three random variables in turbulent annular pipe flow.

Nusselt number

Figure 3(a) illustrate bulk Nusselt (Nu) number compensated with Kays' [11] correlation, $Nu/Re_{Dh}^{0.8}$=$0.021Pr^{0.5}$ for fixed $Pr = 0.71$ (dotted) varies with the Reynolds number Re_{Dh} and radius ratio η. The results indicate that while the influence of curvature (small η) diminishes as Re_{Dh} increases, it remains noticeable even at $Re_{Dh} = 10^6$. **Figure 3(b)** shows local Nusselt numbers $Nu_{i,o}$ at the inner and outer walls for $Re_{Dh} = 17700$. Compared to DNS data [3], ODT provides quality accuracy with maximum errors of 3.17% at the inner wall and 7.01% at the outer wall for $\eta = 0.1$. The curvature effect primarily influences Nu_i, and this influence diminishes as η increases.

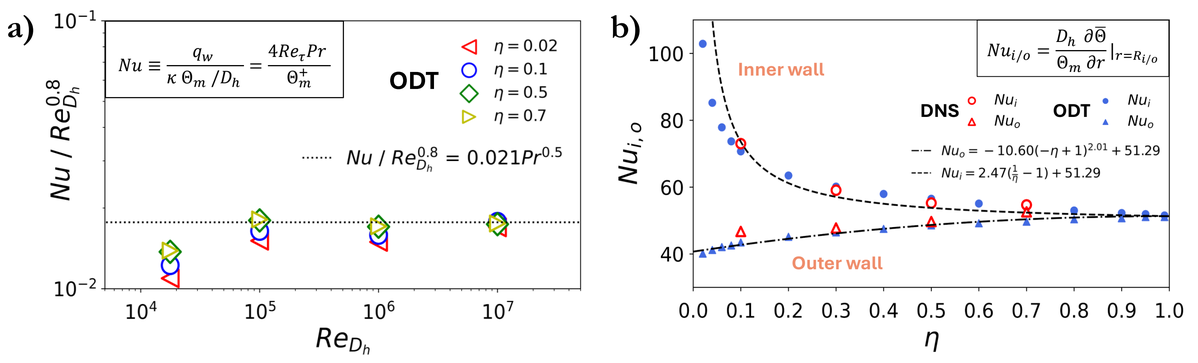

Figure 3: (a) Compensated bulk Nusselt numbers $Nu/Re_{Dh}^{0.8}$ for different Reynolds numbers $Re_{Dh} = 17700 - 10^7$ and radius ratios $\eta = 0.02, 0.1, 0.5, 0.7$ at fixed $Pr = 0.71$. The dotted line indicates an empirical correlation function [11]. **(b)** Gradient-based local Nusselt number Nu_i and Nu_o at the inner and outer cylindrical wall for various radius ratio $\eta = 0.02 - 0.95$ with $Re_{Dh} = 17700$, reproducing and extrapolating reference DNS [3] (red unfilled symbols).

Acknowledgements

This research is supported by the German Federal Government, the Federal Ministry of Education and Research, and the State of Brandenburg within the framework of the joint project EIZ: Energy Innovation Center (project numbers 85056897 and 03SF0693A) with funds from the Structural Development Act for coal-mining regions.

SPONSORED BY THE Federal Ministry of Education and Research

LAND BRANDENBURG

Thermal boundary layers

Figure 4(a) shows that the curvature effect leads to a thinner thermal boundary layer at the inner wall for small η compared to large η. Although ODT slightly underestimates the maximum value of the mean perturbation temperature compared to DNS [3], the model is seemingly able to accurately capture the temperature gradient at the wall. At the outer cylinder wall, the curvature effect on the thermal boundary layer is negligible such that boundary layer profiles align well with the classical law of wall, as shown in **Figure 4(b).** However, at the inner cylinder wall, **Figure 4(c)**, the classical law of the wall increasingly fails to describe the thermal boundary layer as η decreases.

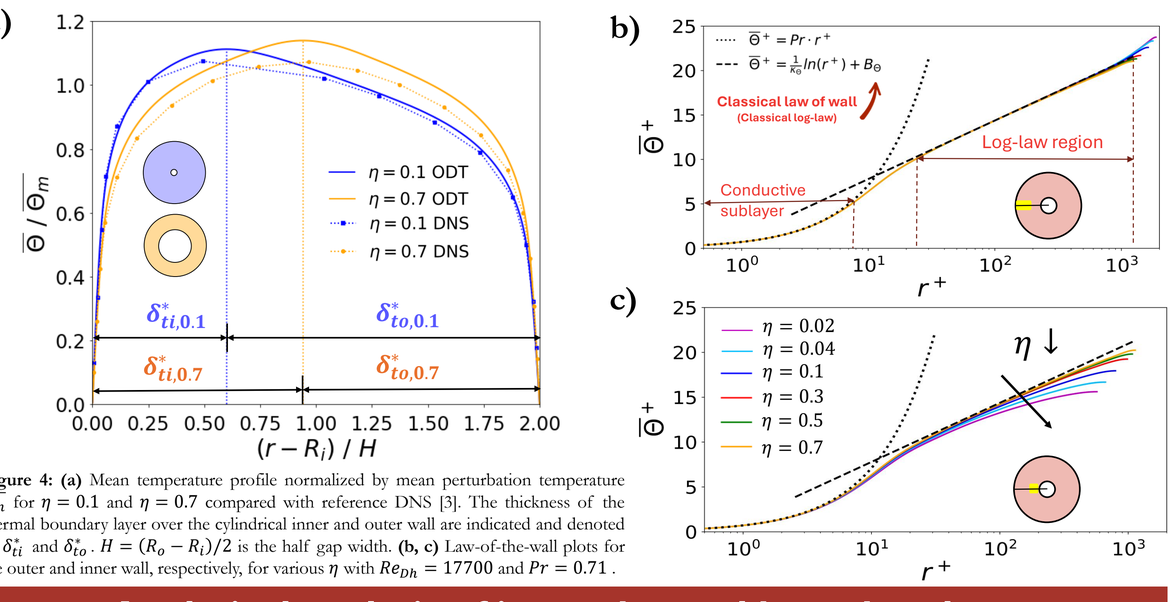

Figure 4: (a) Mean temperature profile normalized by mean perturbation temperature $\overline{\Theta_m}$ for $\eta = 0.1$ and $\eta = 0.7$ compared with reference DNS [3]. The thickness of the thermal boundary layer over the cylindrical inner and outer wall are indicated and denoted by δ^*_{ti} and δ^*_{to} . $H = (R_o - R_i)/2$ is the half gap width. **(b, c)** Law-of-the-wall plots for the outer and inner wall, respectively, for various η with $Re_{Dh} = 17700$ and $Pr = 0.71$.

Analytical analysis of inner thermal boundary layer

We assume that the mean flow is fully developed and axisymmetric. After applying the temporal average to the passive temperature equation (2), re-arranging, and integration over r, yields the turbulent heat flux balance equation as

$$\overline{v'\Theta'} - \alpha\frac{\partial \bar{\Theta}}{\partial r} = r\bar{u}\frac{dT_m}{dx} + \frac{C_1}{r} \text{ , where } C_1 = \frac{1}{\rho C_p}\frac{q_i R_o - q_o R_i}{R_i/R_o - R_o/R_i} \quad (3)$$

Based on the two dominated terms from equation (3), we therefore separated the inner wall thermal boundary layer into a conductive-dominated region and a mixing-length-dominated region, as shown in **Figure 6(a)**.

◆ The conductive-dominated region

- In the region **very close to the inner cylinder**
- $r \approx R_i$ where $r^+ < 10$
- Assume that $\overline{v'\Theta'} \ll \alpha\frac{\partial \bar{\Theta}}{\partial r}$ and $R_i \ll R_o$

Eq. (3) → $\bar{\Theta}^+(r) \approx Pr \cdot R_i^+ \ln\left(\frac{r^+}{R_i^+}\right)$ (4)

◆ The mixing-length-dominated region

- In the region **not close to the inner cylinder** where $r^+ > 10$
- Assume that $\alpha\frac{\partial \bar{\Theta}}{\partial r} \ll \overline{v'\Theta'}$ and $R_i \ll R_o$
- Apply the eddy diffusivity approach $\overline{v'\Theta'} = -\alpha_t\frac{\partial \bar{\Theta}}{\partial r}$

$\alpha_t = \frac{\nu_t}{Pr_t}$ with $\nu_t = \epsilon_1\sqrt{\frac{\tau_i}{\rho}}(r - R_i)$ [12]

Eq. (3) → $\bar{\Theta}^+(r) \approx Pr_t \cdot \frac{1}{\epsilon_1}\ln\left(\frac{r^+ - R_i^+}{r^+}\right) + D_1^+$ (5)

ϵ_1 and D_1^+ are constants, which can be obtained with least square fitting.

Figure 6(d) shows that equation (4) gives an excellent description of the near-wall temperature profile, while equation (5) effectively capture the key statistical features of the turbulent thermal boundary layer on the inner cylinder wall for arbitrary Reynolds number and low Prandtl number. It is noted that the magnitude of turbulent Prandtl number Pr_t is selected differently for $Pr = 0.71$ and $Pr = 0.025$, following common practices. As illustrated in **Figure 6(b,c)**, $Pr_t(Pr)$ is an ODT model prediction that is backed up by evidence through empirical relations.

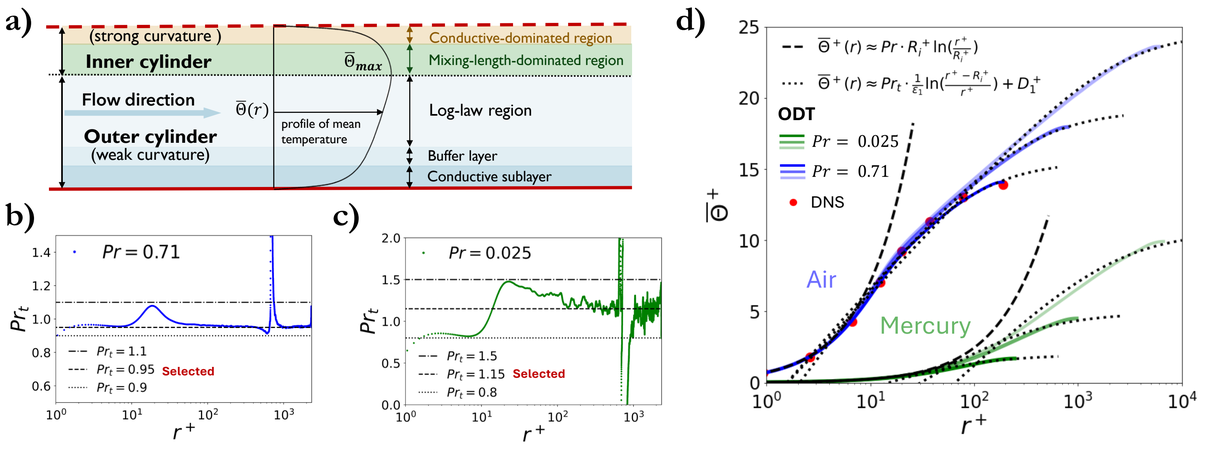

Figure 6: (a) Schematic drawing of different flow regions in the radial gap between the annulus walls. Turbulent Prandtl number for **(b)** $Pr = 0.71$ and **(c)** $Pr = 0.025$. **(d)** Boundary-layer profiles of mean perturbation temperature over cylindrical inner wall with $\eta = 0.1$, Prandtl number $Pr = 0.71$ (blue) and $Pr = 0.025$ (green), and bulk Reynolds number $Re_{Dh} = 17000, 10^5, 10^6$ (colored from dark to light). DNS data [3] is indicated here as red dots for $\eta = 0.1$ and $Re_{Dh} = 17000$. In the conductive-dominated region, $r^+ < 10$ is selected for $Pr = 0.71$, and $r^+ < 15$ for $Pr = 0.025$.

Conclusions

- Curvature effect remains up to high Reynolds number ($Re_{Dh} < 10^7$)
- Rigorous boundary layer analysis extends the classical law of the wall, but requires unknown closure coefficients for annular pipes.
- ODT provides a physically compatible extension to boundary layer analysis due to its predictive capabilities.
- ODT offers a cost-effective and filter-free approach to systematically study boundary layer flows governing the heat transfer in annular pipe flows across various physical parameters, such as η , Re_{Dh}, and Pr, with satisfactory accuracy.

Reference

1 K. Rehme, J. Fluid Mech. **64**, 263–288 (1974).
2 S. Y. Chung and H. J. Sung, Int. J. Heat Fluid Flow **24**(3), 399–411 (2003)
3 E. Bagheri and BC. Wang, Phys. Fluids **33**(5), 055131 (2021).
4 T. Fukuda and T. Tsukahara, Int. J. Heat Fluid Flow **82**, 108555 (2020)
5 M. Ould-Rouiss, L. Redjem-Saad, G. Lauriat, and A. Mazouz, Int. Commun. Heat Mass Transf. **37**(8), 958–963 (2010)
6 M. Ould-Rouiss, L. Redjem-Saad, and G. Lauriat, Int. J. Heat Fluid Flow **30**(4), 578–587 (2009).
7 A. R. Kerstein, J. Fluid Mech. **392**, 277–334 (1999).
8 D. O. Lignell, V. B. Lansinger, J. A. Medina Méndez, M. Klein, A. R. Kerstein, H. Schmidt, M. Fistler and M. Oevermann, Theor. Comput. Fluid Dyn. **32**, 495–520 (2018).
9 M. Klein, H. Schmidt and D. O. Lignell, Int. J. Heat Fluid Flow **93**, 108889 (2022).
10 P. Y. Tsai, M. Klein, and H. Schmidt, PAMM **22**, e202200272 (2023).
11 W. M. Kays, M. E. Crawford, and B. Weigand, Convective heat and mass transfer (Vol.4). New York: McGRAW-Hill.
12 B. J. Boersma and W. P. Breugem, Flow Turbul. Combust. **86**, 113–127 (2011).
13 P. Y. Tsai, M. Klein, and H. Schmidt, PAMM **23**, e202300167 (2023).